New Architecture of Optical Interconnect for High-Speed Optical Computerized Data Networks (Nonlinear Response)

El-Sayed A. El-Badawy

Alexandria Higher Institute of Engineering &Technology, Alexandria 21311, Egypt.
Senior Member IEEE, Member of the Optical Society of America (OSA), E-mail: sbadawy@ieee.org

Farag Z. El-Halafawy

Elect. and Comm. Eng. Dept., Faculty of Electronic Engineering, Menoufia Univ., Menouf 32951, Egypt.
Member of the Optical Society of America (OSA) and the Intern. Society of Optical Engineering (SPIE)

Hamdy A. Kelash **Ashraf. M. Abou-Tabl**

Computer Science and Eng. Dept., Faculty of Electronic Engineering, Menoufia Univ., Menouf 32951, Egypt

ABSTRACT

Although research into the use of optics in computers has increased in the last and current decades, the fact remains that electronics is still superior to optics in almost every way. Research into the use of optics at this stage mirrors the research into electronics after the 2nd World War. The advantages of using fiber optics over wiring are the same as the argument for using optics over electronics in computers. Even through totally optical computers are now a reality, computers that combine both electronics and optics, electro-optic hybrids, have been in use for some time.

In the present paper, architecture of optical interconnect is built up on the bases of four Vertical-Cavity Surface-Emitting Laser Diodes (VCSELD) and two optical links where thermal effects of both the diodes and the links are included. Nonlinear relations are correlated to investigate the power-current and the voltage-current dependences of the four devices. The good performance (high speed) of the interconnect is deeply and parametrically investigated under wide ranges of the affecting parameters. The high speed performance is processed through three different effects, namely the device 3-dB bandwidth, the link dispersion characteristics, and the transmitted bit rate (soliton). Eight combinations are investigated; each possesses its own characteristics. The best architecture is the one composed of VCSELD that operates at 850 nm and the silica fiber whatever the operating set of causes. This combination possesses the largest device 3-dB bandwidth, the largest link bandwidth and the largest soliton transmitted bit rate. The increase of the ambient temperature reduces the high-speed performance of the interconnect

I. Introduction

Although research into the use of optics in computers has increased during the last and current decades, the fact remains that electronics is still superior to optics in almost every way.

The main problems facing the development of the optical computer is related to one of its main benefits. Because photons do not interact with each other like electrons, it is still necessary to include transistors that perform a switch-on or -off on the signal. Until researchers can develop an optical switch that will perform the same functions as a transistor, the development of optical computer will remain a thing of the future [1].

References [2, 3] presented an approach to model the optical interconnect used in networks and advanced high-performance computing systems. The model is generic enough that it can be applied to fiber or free-space technologies, yet precise enough to extract from it salient performance predictions. The developed model was intended as an analysis tool for system builders, and to provide a guide for developing upcoming technologies such as free-space smart pixel-based interconnects [2-4].

The reason of optical interconnects are not widely implemented in modern computing systems is due to computer architecture design and how interconnects are balanced within those constraints.

In Section II, we cast a basic model and a parametrical nonlinear analysis of optical interconnections based on two basic sets of elements namely; VCSELDs as sources, and polymer fiber and silica fiber as links. Thermal effects are considered as well as the spectral dependence. Our goal is the maximization of bandwidths of the two basic sets of elements, namely eight structures will be processed.

II. Basic Model, Governing Equations and Analysis

II.1. Optical sources [5]

The first device is an index-guided, vertically-contacted VCSELD. The device has a 100 μm^2 area and is composed of GaAs-AlAs DBR mirrors, three $In_{0.2}Ga_{0.8}As$ quantum wells, and $Al_{0.2}Ga_{0.8}As$ confinement layers. Lateral carrier confinement is provided through an etched mesa design. The second device is an AlGaInP-based 683 nm selectively-oxidized VCSELD with a 3 μm x3 μm area. This device consists of compressively-strained InGaAs graded DBR's. The third device is 863 nm bottom emitting AlGaAs

VCSELD. This 16 μm diameter device was grown on an $Al_{0.1}Ga_{0.9}As$ n-type DBR, six quantum wells, and a C-doped $Al_{0.15}Ga_{0.85}As$-AlAs, GaAs-$Al_{0.2}Ga_{0.8}As$ n-type DBR, six quantum wells, and a C-doped $Al_{0.15}Ga_{0.85}As$-$Al_{0.5}Ga_{0.5}As$-AlAs p-type DBR. The final device is the VCSEL a 3.1 μm diameter, thin oxide apertured device composed of an $Al_{0.9}Ga_{0.1}As$-GaAs p-type DBR, three $In_{0.1}$-$Ga_{0.83}As$-GaAs quantum wells, and an $Al_{0.3}Ga_{0.7}As$ cavity

In the present paper, we cast the following more accurate nonlinear relationships than that of [6] to account for voltage-current (V-I) and output power-current (P_o-I) dependences over the temperature range $290 \le T, K \le 310$ under the forms:

$$P_o = a + bI + cI^2 \text{, mW} \tag{1}$$

$$V = \alpha + \beta I + \gamma I^2 \text{, V} \tag{2}$$

We have computed the two sets of the coefficients based on [7,8].

Table I Coefficients of Eqs. (1) and (2)

Device	λ, nm	a	b	c	α	β	γ
InGaAs	980	0.05	0.24	-0.004	1.1	0.1760	0.015
AlGaInP	683	-0.11	0.19	-0.0035	1.9007	0.1300	0.025
AlGaAs	863	-0.5260	0.23	-0.005	2.2400	0.0600	-0.01
AlGaAs	850	0.21	0.28	-0.015	2.1	0.51	-0.02

Table II [5,7,8]

Parameters resulting from the fitting of the VCSELD model to experimental data for four devices:
(a) Index-guided InGaAs VCSELD, (b) Selectively oxidized AlGaInP VCSELD, (c) Bottom-emitting AlGaAs VCSELD, and (d) Thin oxide apertured VCSELD

Parameters	(a)	(b)	(c)	(d)
$G_o(s^{-1})$	2.112×10^4	6.509×10^4	1.6×10^4	8.486×10^5
N_{to}	2.206×10^7	6.208×10^6	1.943×10^6	1.286×10^6
I_{1o}(A), mA	3.935×10^3	22.44×10^3	2.073×10^3	1.923×10^4
a_0(K)	3700	6773	3016	2422
a_1(K)	1.259×10^{-5}	1.980×10^{-4}	1.799×10^{-6}	8.465×10^{-6}
a_2	1.259×10^{-5}	9.377×10^{-9}	1.854×10^{-8}	5.570×10^{-8}
a_3(K)	2.471×10^9	6.634×10^8	7.662×10^8	7.472×10^9
λ,nm	980	683	863	850
η_i	1.0	1.0	1.0	1.0
τ_{no}(ns)	3	3	5	1.201
τ_{p0}(ps)	2.989	2.455	2.280	2.884
ε_{oo}	0	1.79×10^{-6}	0	3.497×10^{-6}
R_{th}(°C/mW)	1.647	5.5	1.6	0.896

The leakage current I_ℓ is given by:

$$I_\ell = I_{\ell o} \exp\left[\left(-a_o + a_1 N_o + a_2 N_o T - \frac{a_3}{N_o}\right)/T\right] \tag{3}$$

where the parameters $I_{\ell o}$, a_o, a_1, N_o, a_2, and a_3 are given in Table II.

Based on the models of [5, 7], the device bandwidth BW_s is an electro-thermal quantity and is cast [9-12] under the form:

$$BW_s(I,T) = \omega_r \sqrt{1 + \sqrt{1 + 3(\omega_o/\omega_r)^4}} \tag{4}$$

with

$$\omega_r = \sqrt{\omega_o^2 - 0.5B^2} \tag{5}$$

where BW_s, ω_r, ω_o, and B take their usual definitions as in [9-12]. In fact, these quantities are functions of I_o, T, and the physical parameters of the devices; also, BW_s is a good criterion for the device speed.

II.2. The optical links

A. Polymer link

Based on the models of [13-16], the dispersion characteristics depend on the refractive index, where usually, index measurements are fit to the three-term Sellmeier dispersion relation.

The total chromatic dispersion and modal dispersion in multi-mode fibers of radius R are given by [14, 15]:

$$D_{tp} = (M_{mat} + P) = f_{ch}(\lambda, T, R) \tag{6}$$

$$D_{mod} = f_{mod}(\lambda, T, R, \Delta) \tag{7}$$

where D_{tp} is the total chromatic dispersion coefficient, ps/nm.km, M_{mat} is the material dispersion coefficient, ps/nm.km, P is the profile dispersion coefficient, ps/nm.km, D_{mod} is the modal dispersion coefficient, and Δ is the relative refractive index difference.

The polymer bandwidth is given by:

$$BW_p = 0.44/(D_{tp}\Delta\lambda R_s) \text{, THz} \tag{8}$$

Also, two transmitted bit rates based on the model of [16], the soliton bit rate is computed as:

$$B_s^{-2} P_s = 59.6(\lambda/1.54)^3 (A_e/20)(3.2x10^{-20}/n_{nl}) D_t \text{ ,W/Tbit}^2 \tag{9}$$

where B_s is the soliton bit rates, P_s is power /bit, A_e is the effective area, μm^2 , n_{nl} is nonlinear refractive index coefficient, and D_t is the dispersion coefficient in ps/nm.km

B. Binary silica fiber link

Following the spirit of [17,18], in separating the various contributions to the total chromatic dispersion in monomode silica doped fibers of radius R, we have:

$$D_{tf} = \Delta\tau/\Delta\lambda = -(M_{md} + M_{wd}) \tag{10}$$

where M_{wd} is the waveguide dispersion coefficient in ps/nm.km, and M_{md} is the material dispersion coefficient in ps/nm.km.

The transmitted soliton bit rate is computed as in Eq. (9). The silica fiber bandwidth BW_f is given as:

$$BW_f = 0.44/(D_{tf}\Delta\lambda R_s) \tag{11}$$

One item of special interest is the link bandwidth-link length product P_R where,

$P_{RP} = BW_P.R_s$, and (12)

$P_{RF} = BW_f.R_s$ (13)

Thus, our basic model is terminated. In Section III, we will investigate variations of the set of causes {BW_f, BW_p, , P_{RP}, P_{RF}, B_{SF}, B_{SP}} against variations of the set of effects {I, T, R_s, R_{df}, Δ, Δλ} over wide ranges of the affecting parameters.

III. Results and Discussion

Causes of any architecture are in the following set {T, I, R, Δ, R_s} where these causes are, respectively, the ambient temperature, the injected current, the fiber radius, the relative refractive index difference, and the link length.

While effect of any architecture are in the following set $\{f_{3\text{-dB}}$, BW, $B_{rs}\}$ where these effects are, respectively, the device 3-dB bandwidth, the link bandwidth, and the transmitted soliton bit rate.

III.1. Variations of the Four Device and Two Links Characteristics

Samples of variations of the four devices characteristics against variations of the affecting parameters are displayed in Fig.1-20, where the following features are clarified: i) Whatever the device is, $f_{3\text{-dB}}$ and I_o are in positive correlations, ii) Whatever the device is, $f_{3\text{-dB}}$ and T_o are in negative correlations, iii) The fourth device (thin-oxide-aperture of composed structure, λ=0.85 µm is the faster device, where it possesses $f_{3\text{-dB}}$ over the range from 16 GHz up to 35 GHz at room temperature 290 K., iv) The silica bandwidth BW_f is greater than that of polymer fiber for any device (λ=0.98, 0.683, 0.863, and 0.85 µm), and v) The soliton transmitted bit rates are consequently greater in silica fibers than that of polymer fibers. In general, both BW_{rp} and B_{rsp} decrease as Δ increases.

Variations of both BW_p and BW_f against variations of the link length R_s are given, where both the two bandwidths and link length possess negative correlations. As known before, the soliton bit rates are link length-independent quantities. Finally, an increase in the link radius reduces the transmitted bit rates due to the increase in the effective area..

III.2. Comparison of the Eight Architectures

In the following table, we summarize the maximum possible features of the eight architectures over the total obtained results: The summarized results, in Table III, indicate that: i) The fourth device (λ =0.85 µm) is the faster device, and ii) The link made of silica fiber possesses the largest bandwidth and consequently the maximum possible soliton bit rate. Thus, the architecture made of VCSELD of λ = 0.85 µm with the link made of silica is the best architecture.

λ_R=0.98 µm, Dn=0.0075,	**T_O=290 K, Δλ=0.5E-4 µm**	**Rp=750 µm, D1**		**λ_R=0.683 µm, Dn=0.0075,**	**T_O=290 K, Δλ=0.5E-4 µm**	**Rp=750 µm, D2**

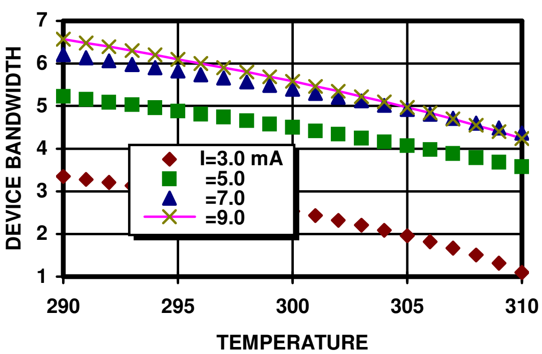

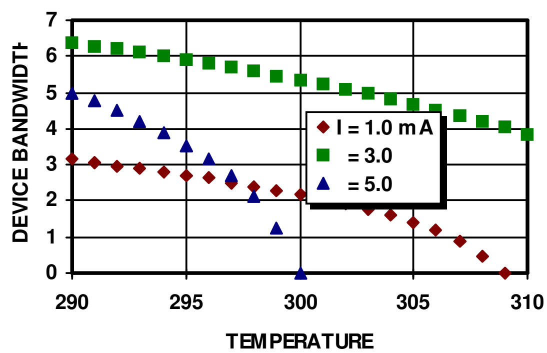

Fig.1. Variations of device bandwidth, $F_{3\text{-dB}}$, GHz against Temperature, T, K at the assumed set of parameters.

Fig.2. Variations of device bandwidth, $F_{3\text{-dB}}$, GHz against Temperature, T, K at the assumed set of parameters

λ_R=0.863 µm, Dn=0.0075,	**T_O=290 K, Δλ=0.5E-4 µm**	**Rp=750 µm, D3**		**λ_R=0.85 µm, Dn=0.0075,**	**T_O=290 K, Δλ=0.5E-4 µm**	**Rp=750 µm, D4**

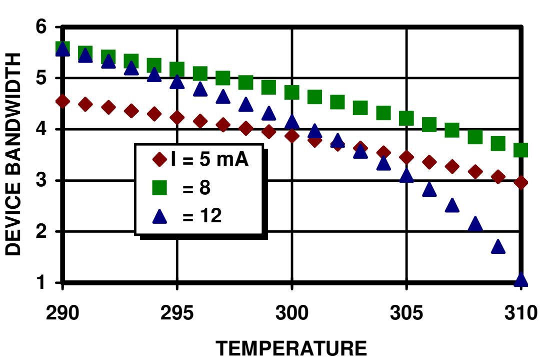

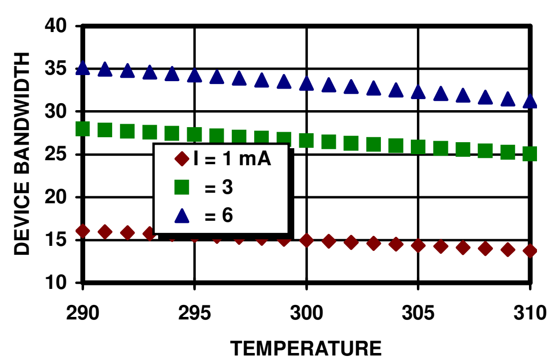

Fig.3. Variations of device bandwidth, $F_{3\text{-dB}}$, GHz against Temperature, T, K at the assumed set of parameters.

Fig.4. Variations of device bandwidth, $F_{3\text{-dB}}$, GHz against Temperature, T, K at the assumed set of parameters

λ_R=0.863 μm, Dn=0.0075,	T_O=290 K, Δλ=0.5E-4 μm	Rp=750 μm, D3		λ_R=0.85 μm, Dn=0.0075,	T_O=290 K, Δλ=0.5E-4 μm	Rp=750 μm, D4

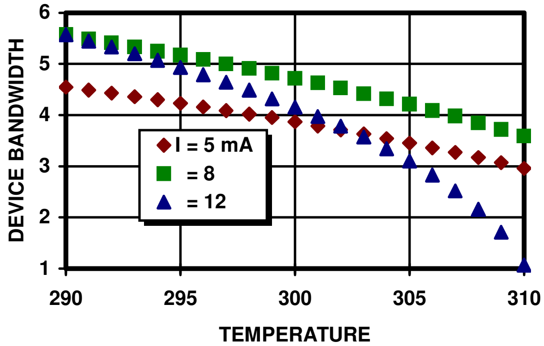

Fig.3. Variations of device bandwidth, $F_{3\text{-dB}}$, GHz against Temperature, T, K at the assumed set of parameters.

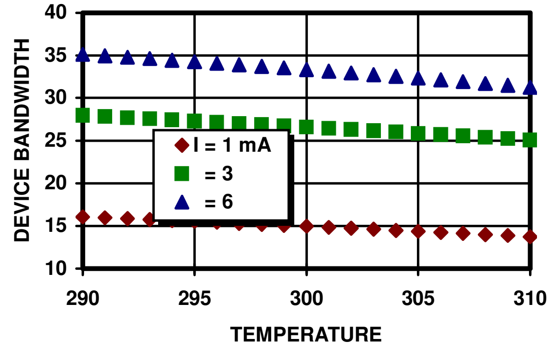

Fig.4. Variations of device bandwidth, $F_{3\text{-dB}}$, GHz against Temperature, T, K at the assumed set of parameters

λ_R=0.98 μm,	T_O=290 K,	Rp=750 μm,	Dn=0.0075,	Δλ=0.5E-4 μm

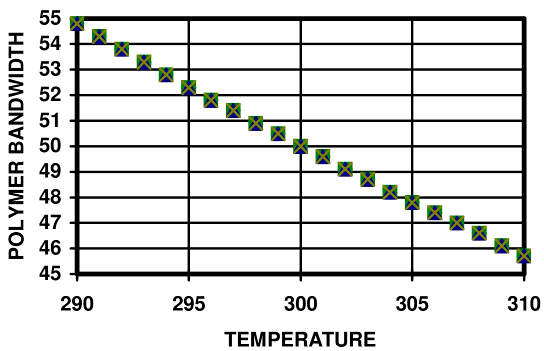

Fig.5. Variations of polymer bandwidth, BW_P, GHz against temperature, K at the assumed set of parameters

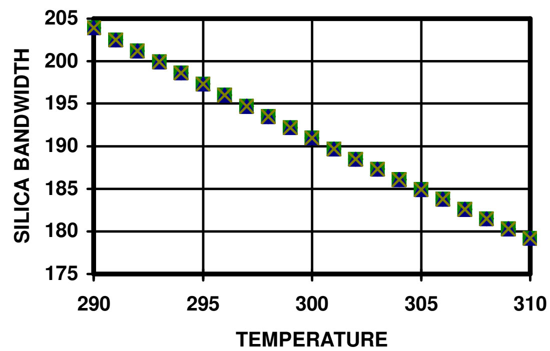

Fig.6. Variations of silica bandwidth, BW_F , GHz against temperature, T, K at the assumed set of parameters.

λ_R=0.98 μm,	T_O=290 K,	Rp=750 μm,	Dn=0.0075,	Δλ=0.5E-4 μm

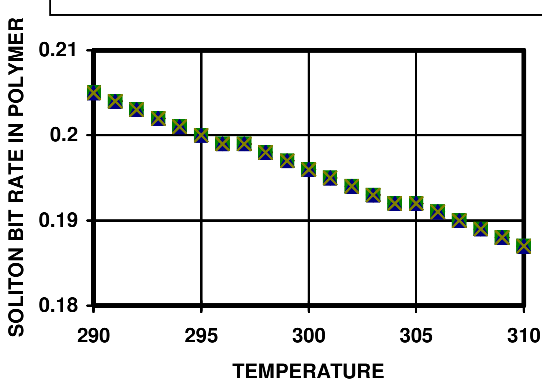

Fig.7. Variations of soliton bit rate in polymer, B_{RSP}, Gb/s against temperature, T, K, at the assumed set of parameters.

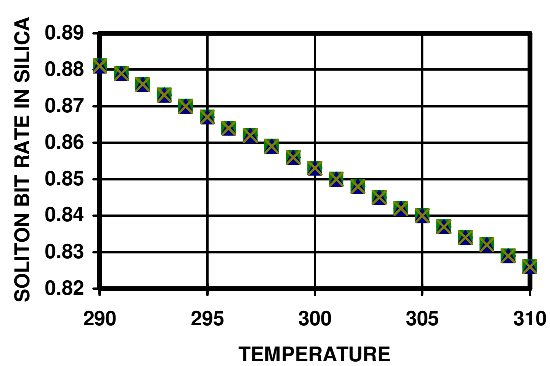

Fig 8. Variations of soliton bit rate in silica,B_{rsf}, Gb/s against temperature, T, K at the assumed set of parameters

λ_R=0.683 µm,	T_O=290 K,	Rp=750 µm,	Dn=0.0075,	$\Delta\lambda$=0.5E-4 µm

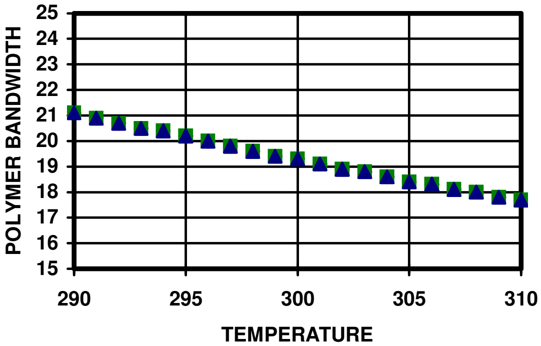

Fig.9. Variations of polymer bandwidth, BW_P, GHz against Temperature, K at the assumed set of parameters

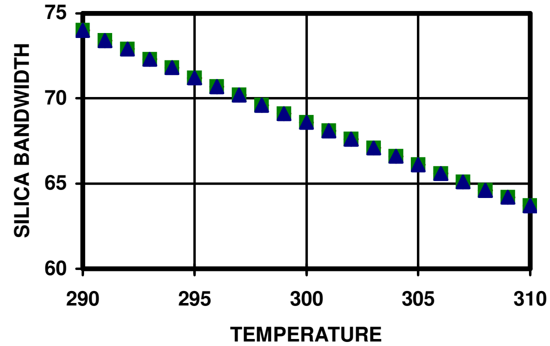

Fig.10. Variations of silica bandwidth, BW_F , GHz against temperature, T, K at the assumed set of parameters.

λ_R=0.683 µm,	T_O=290 K,	Rp=750 µm,	Dn=0.0075,	$\Delta\lambda$=0.5E-4 µm

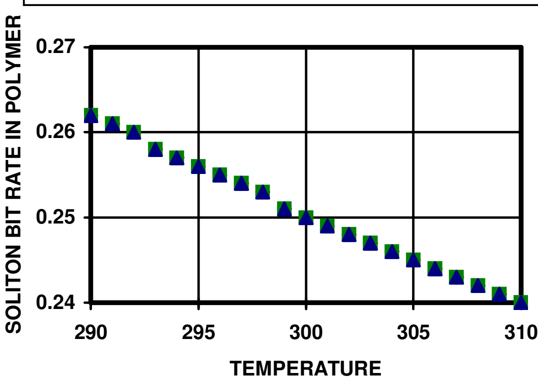

Fig.11. Variations of soliton bit rate in polymer, B_{RSP}, Gb/s against temperature, T, K, at the assumed set of parameters.

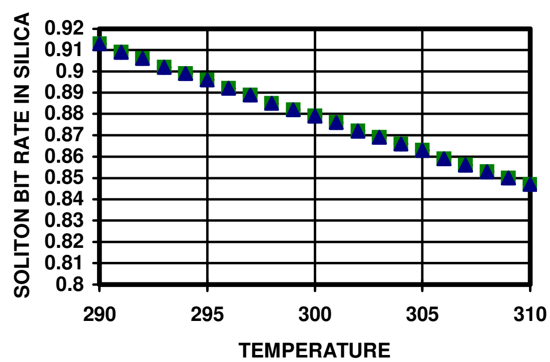

Fig 12. Variations of soliton bit rate in silica,B_{rsf}, Gb/s against temperature, T, K at the assumed set of parameters

λ_R=0.863 µm,	T_O=290 K,	Rp=750 µm,	Dn=0.0075,	$\Delta\lambda$=0.5E-4 µm

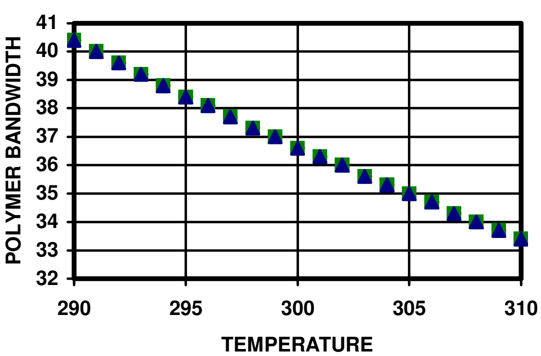

Fig.13. Variations of polymer bandwidth, BW_P, GHz against Temperature, K at the assumed set of parameters

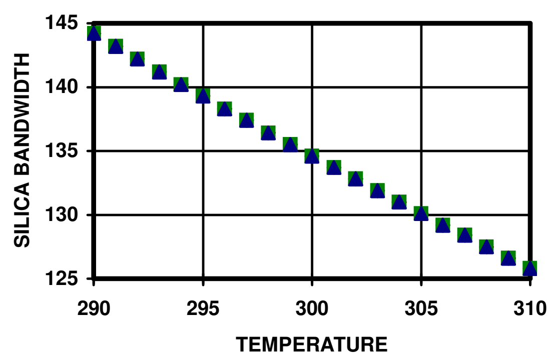

Fig.14. Variations of silica bandwidth, BW_F , GHz against temperature, T, K at the assumed set of parameters.

λ_R=0.863 µm, T_O=290 K, Rp=750 µm, Dn=0.0075, $\Delta\lambda$=0.5E-4 µm

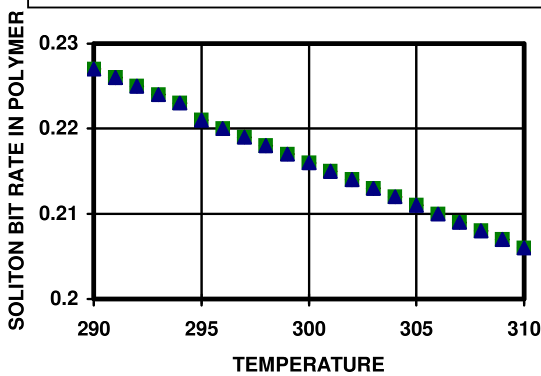

Fig.15. Variations of soliton bit rate in polymer, B_{RSP}, Gb/s against temperature, T, K, at the assumed set of parameters.

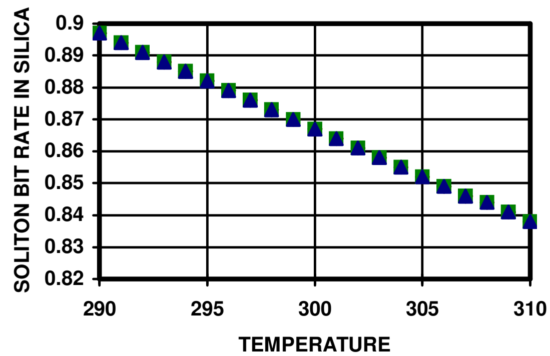

Fig 16. Variations of soliton bit rate in silica,B_{rsf}, Gb/s against temperature, T, K at the assumed set of parameters

λ_R=0.85 µm, T_O=290 K, Rp=750 µm, Dn=0.0075, $\Delta\lambda$=0.5E-4 µm

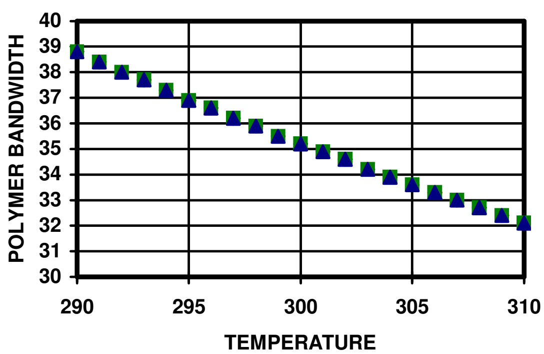

Fig.17. Variations of polymer bandwidth, BW_P, GHz against Temperature, K at the assumed set of parameters

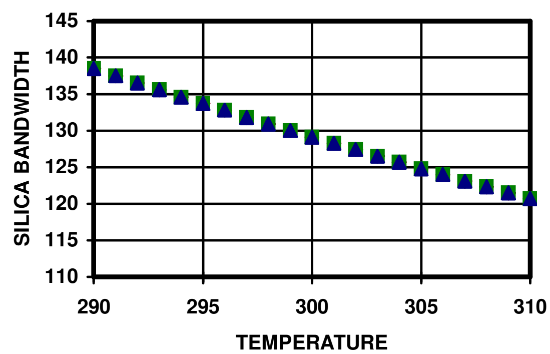

Fig.18. Variations of silica bandwidth, BW_F , GHz against temperature, T, K at the assumed set of parameters.

λ_R=0.85 µm, T_O=290 K, Rp=750 µm, Dn=0.0075, $\Delta\lambda$=0.5E-4 µm

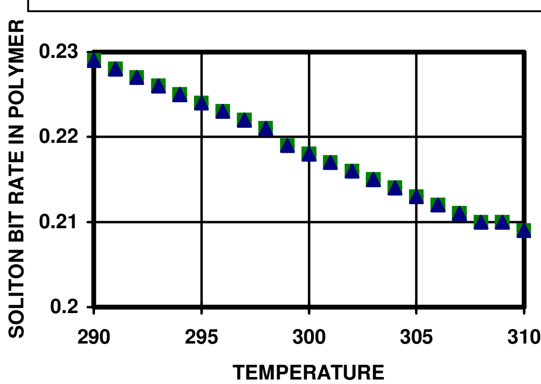

Fig.19. Variations of soliton bit rate in polymer, B_{RSP}, Gb/s against temperature , T, K, at the assumed set of parameters.

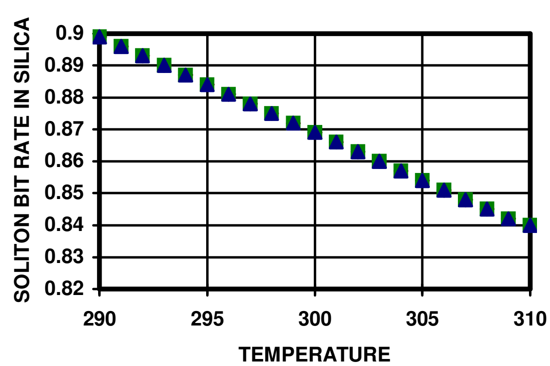

Fig 20. Variations of soliton bit rate in silica,B_{rsf}, Gb/s against temperature, T, K at the assumed set of parameters

IV. Conclusions

A special software program is cast to handle the architecture of optical interconnect for high-speed optical data networks. The design is based on four optical VCSEL diodes of different structures and different operating wavelengths λ_s=980 nm, 683 nm, 863 nm, and 850 nm. Also, the design handles two fiber links made of either PMMA polymer or silica fibers. Thus, we have investigated eight different designs, where special emphasis is focused on the following causes and effects shown in Fig.21.

Fig.21. Causes and effects in the design of OI

a. **Causes are:** i) The injected current I, mA. ii) The ambient temperature T_o, K., iii) The link radius R_p (for polymer) and R_f (for silica, μm)., iv) The link length, R_s, km., and v) The relative refractive index difference, Δ.
b. **The effects are**: i) The device 3-dB bandwidth, $f_{3\text{-dB}}$, GHz.**,** ii) The links bandwidths, BW_p, BW_f, GHz., and iii) The soliton transmitted bit rate, B_{rsp}, B_{rsf}, Gb/s.

Each device has its own thermal and electrical characteristics, also each of the two links has its thermal and spectral characteristics.

Based on the model of Section II and the obtained results in Section III, the following conclusions are made: i) The four devices 3-dB bandwidths $f_{3\text{-dB}}$, and the injected current I_o possess positive correlations, while $f_{3\text{-dB}}$ and T_o possess negative correlations, ii) Thin-film oxide VCSELD (λ=850 nm) is the one of highest speed, iii) Both the two links bandwidths (BW_p and BW_f) and the soliton bit rates.(B_{rsp}, B_{rsf}) and the ambient temperature, T_o possess negative correlations, iv) Soliton bit rates using silica fibers are larger than that of polymer fibers. The fourth device, that operates at (λ=850 nm), yields the largest bandwidth, and consequently the maximum soliton bit rate, v) (BW_p, B_{rsp}) and the relative refractive index difference Δ have negative correlations, while (BW_f, B_{rsf}) and Δ have positive correlations, vi) (BW_p, BW_f) and the link length R_s possess negative correlations, of course, both $B_{rsp,}$ and B_{rsf} are link-length-independent quantities, and vii) Finally, the increasing link radius (R_p or R_f) reduces the transmitted bit rate.

Table III: Comparison of the eight architectures

λ, μm	**$F_{3\text{-dB}}$, GHz**	**$BW_{f,}$ GHz**	**B_{rsf}, Gb/s**	**$BW_{p,}$ GHz**	**B_{rsp}, Gb/s**
0.98	**6.55**	**204**	**0.881**	**54**	**0.204**
0.683	**6.35**	**73.5**	**0.914**	**21**	**0.262**
0.863	**5.7**	**144**	**0.897**	**40.4**	**0.227**
0.85	**34.9**	**138**	**0.898**	**38.8**	**0.228**

References

[1] N. M. Jokerest, M. A. B., S.-Y. Cho, S. Wilkinson, and D. S. Wills, "The Heterogenous Integration of Optical Interconnects into Integrated Microsytems," IEEE J. of Selected Topics in Quantum Electronics, Vol. 9, No. 2, pp. 350-360, March/April 2003.

[2] S. Shimada and T. Matsumoto, "Very-high-Speed Optical Signal Processing," Proceedings of the IEEE, Vol. 81, No. 11, pp. 1633-1646, Nov. 1993.

[3] A. Z. Shang and F. A. P. Tooler, "Digital Optical Interconnects for Networks and Computing Systems," J. of Lightwave Technol., Vol. 18, No. 12, pp. 2086-2094, Dec. 2000.

[4] D. Huang, R. Lytel and H. L. Davison, "Optical Interconnects: Out of the Box Forever," IEEE J. of Selected Topics in Quantum Electronics, Vol. 9, No. 2, pp. 614-623, March/April 2003.

[5] P. V. Mena, J. J. Morikuni, S. M. Kang, A. V. Harton, and K. W. Wyatt, "A Comprehensive Circuit-Level Model of Vertical-Cavity Surface Emitting Lasers," J. Lightwave Technol., Vol. 17, No. 12, pp. 2612-2632, Dec. 1999.

[6] Hamdy M. Kelash and Ashraf M. Abou-Tabl, "New Architecture of Interconnect for High–Speed Optical Computerized Data Networks," Accepted for publication in MJEER, Vol.17, No.2, F of EE, Menouf, EGYPT, July 2007

[7] J. P. V. Mena, J. J. Morukuni, S. M. Kang, A. V. Harton, and K. W. W.yatt, "A Simple Rate Equation Based Thermal VCSEL Model, "J. Lightwave Technol., Vol. 17, No. 5, pp. 865-872, May. 1999.

[8] I. P. Kaminouv and T. L. Koch, *Optical Fiber Telecommunication IIIB*, Chapter 6 by L.A. Coldren and B. J. Thibeault, Vertical-Cavity Surface-Emitting Lasers, pp.200-266, AP USA, 1997.

[9] Hamdy M. Kelash, "Thermal Penalties and Sensitivities in Supercomputer High Performance Computing," AUEJ 2002 Fac. of Eng., Al-Azhar University, Cairo-Egypt, Vol.5, No. 2, April 2002.

[10] Hamdy M. Kelash, Hoda S. Sorour, and Nabila El-Halafawy, "High-Speed Optical Computing Devices Based on VCSEL Diodes with Feedback," AUEJ 2002 Fac. of Eng., Al-Azhar University, Cairo-Egypt, Vol.7, No. 3, pp.324-333, July 2004.

[11] Hamdy M. Kelash, "Modeling and Simulation of High Speed Optical Computing Devices: On Transient Response and Rise Time," MJEER, Vol.13, No. 1, pp.105-121, F of EE Menouf, Egypt, Jan 2003.

[12] Hamdy M. Kelash, "High-Speed Photonic Devices in High Performance Computing," AUEJ 2002 Fac. of Eng., Al-Azhar University, Cairo-Egypt, Vol.5, No. 1, Jan 2002.

[13] G. D. Brown, "Bandwidth and Rise Time Calculations for Digital Multimode Fiber-Optic Data Links," J. Lightwave Technol., Vol. 10, No. 5, pp. 672-678, May. 1992.

[14] J. Zubia and J. Arrae, "Plastic Optical Fibers: An Introduction to Their Technological Processes and Applications," Optical Fiber Technology, Vol.7, pp.101-140, 2001.

[15] I. Ishigure, M. Sato, A. Kondo, and Y. Koike, "High Bandwidth Graded Index Polymer Optical Fiber with High-Tempeature Stability," J. Lightwave Technol., Vol. 20, No. 8, pp. 1443-1448, Aug. 2002.

[16] E. Disurve, *Erbium-Doped Fiber Amplifiers : Principle and Applications*, J. W & Sons, Inc., NY, USA, 1994.

[17] W. Flemming," Dispersion in GeO_2-SiO_2 Glasses," Applied Optics, Vol.23, No.24, pp.4486-4493, Dec.1984.

[18] G. Keiser, *Optical Fiber Communications*, 3rd Ed., McGraw-Hill Higher Education, Chapter 3, USA, 2000.